BMC Biology

RESEARCH

Open Access

Juvenile hormone signaling is indispensable for late embryogenesis in ametabolous and hemimetabolous insects

Ya-Nan Lv[1†], Mei Zeng[1†], Zi-Yu Yan[1†], Pei-Yan Zhang[1], Ning Ban[1], Dong-Wei Yuan[1], Sheng Li[1,2*], Yun-Xia Luan[1,2*] and Yu Bai[1,2*]

Abstract

Background Juvenile hormone (JH) is an insect-exclusive hormone involved in regulating diverse aspects of insect physiology, and the evolution of its diverse function is widely interesting. Studying embryogenesis in basal wingless insects is important to understand the functional evolution of JH; however, experimental studies in this regard are scarce. In this study, we conducted CRISPR/Cas9-mediated knockout (KO) of genes involved in JH biosynthesis and signaling cascades in the ametabolous firebrat, *Thermobia domestica*. Additionally, we investigated whether the primitive action of JH is conserved in the hemimetabolous cricket, *Gryllus bimaculatus*.

Results We observed that KO of *JHAMT*, *CYP15A1*, *Met*, and *Kr-h1* resulted in embryonic lethality in *T. domestica*. Deprivation of JH or JH signaling arrested the progression of extraembryonic fluid resorption after dorsal closure and hatching, which is consistent with the gene expression pattern showing high *Kr-h1* expression in the late embryos of *T. domestica*. The embryos deficient in JH signaling displayed wrinkled and weak legs. Comparative transcriptome analysis revealed that JH signaling promotes embryonic leg maturation through inducing energy supply and muscle activity, as validated by transmission electron microscopy (TEM). In addition, JH signaling exhibited similar embryonic effects in *G. bimaculatus*.

Conclusions This study reveals the indispensable role of JH signaling in facilitating the maturation of terminal tissues during late embryogenesis, as demonstrated by the regulation of leg development, in ametabolous and hemimetabolous insects. These findings further indicate that the embryonic functions of JH evolved earlier than its anti-metamorphic functions during postembryonic development.

Keywords JH, Embryogenesis, Ametaboly, Hemimetaboly, Leg, Muscle

[†]Ya-Nan Lv, Mei Zeng and Zi-Yu Yan contributed equally to this work.

*Correspondence:
Sheng Li
lisheng@scnu.edu.cn
Yun-Xia Luan
yxluan@scnu.edu.cn
Yu Bai
yubai@m.scnu.edu.cn
[1] Guangdong Provincial Key Laboratory of Insect Developmental Biology and Applied Technology, Guangzhou Key Laboratory of Insect Development Regulation and Application Research, Institute of Insect Science and Technology, School of Life Sciences, South China Normal University, Guangzhou 510000, China
[2] Guangmeiyuan R&D Center, Guangdong Provincial Key Laboratory of Insect Developmental Biology and Applied Technology, South China Normal University, Meizhou 514000, China

Background

Juvenile hormone (JH) plays crucial roles in insect metamorphosis [21–23, 29], reproduction [31, 35, 45], phenotypic plasticity [4], sexual behavior [11], and various other physiological activities. From a molecular perspective, the methylation reaction catalyzed by juvenile hormone acid methyltransferase (JHAMT) and the oxidation reaction catalyzed by cytochrome P450 15A1 (CYP15A1) are pivotal steps in the biosynthesis of JH III, which is the most prevalent and predominant JH homolog in insects [18]. JH exerts its regulatory function upon binding to the intracellular receptor methoprene-tolerant (Met) [22, 23, 26]. Subsequently, the JH-Met complex directly induces the expression of*Krüppel homolog 1* (*Kr-h1*), a major transcription factor representing JH signaling [25, 33].

The main modes of postembryonic development in insects are ametaboly, hemimetaboly, and holometaboly. Ametaboly is considered the most "ancestral" mode from which hemimetaboly evolved, followed by the evolution of holometaboly [7, 8]. Ametabolous and hemimetabolous species hatch as juveniles/nymphs morphologically similar to adults, while holometabolous insects produce an "incompletely developed" larva and they have an additional pupal stage [38]. Insect embryogenesis mainly comprises segmentation (early stage), morphogenesis and growth (middle stage), and differentiation and maturation (late stage), delineated by germ band formation and dorsal closure, respectively [12]; Truman et al., [39]).

While the role of JH signaling during postembryonic development is well-characterized, its function during embryonic development remains poorly understood. Embryonic development is generally less dependent on JH signaling in holometabolous insects, such as the fly *Drosophila melanogaster* [1, 30, 42], the mosquito*Aedes aegypti* [46], and the silkworm*Bombyx mori* [13]. However, exceptions to this trend include a parental knockdown analysis of the JH receptor Met in the holometabolous beetle*Tribolium castaneum*, which indicated the importance of Met from mid to late embryogenesis in this insect species [34]. In contrast, JH signaling is universally essential during embryogenesis in ametabolous and hemimetabolous insects. In the migratory locust*Locusta migratoria*, the late embryos are highly susceptible to the anti-allatin effect (chemical destruction of the corpora allata where JH is synthesized) of the precocene [2]. JH application treatment has suggested that its role in post dorsal closure and inducing the nymphal cuticle in the cricket*Acheta domesticus* [16]. Similarly, the use of maternal RNAi treatments to knockdown transcripts of components of the JH synthesis and response pathways in the German cockroach*Blattella germanica*also interfered with late embryonic development, although some early embryonic anomalies were noted as well [17]. Besides, recent pharmacological experiments have demonstrated the crucial role of JH in promoting terminal differentiation and maturation during late embryogenesis in the ametabolous firebrat*Thermobia domestica* [39]. Despite these observations, genetic evidence and molecular mechanisms of JH actions during embryonic development in ametabolous and hemimetabolous insects are still lacking.

Evolutionary developmental biology (evo-devo) studies of JH regulatory roles during embryogenesis will provide valuable insight into the evolution of insect metamorphosis. The ametabolous *T. domestica* and the hemimetabolous *Gryllus bimaculatus*, one of the best studied hemimetabolous insects with well-characterized embryogenesis [15], could be used as appropriate model insects for evo-devo studies. The limb, such as the thoracic leg, has long served as a paradigm for studying embryonic pattern formation and evolutionary diversification. During leg differentiation and maturation, a variety of distinct tissue types, mainly including cuticles (exoskeletons), muscles, and nerves, are patterned and subsequently must be integrated to form coherent functional units [32].

In this study, CRISPR/Cas9-mediated gene knockout (KO) in *T. domestica* showed that the generation 0 (G0) mutants (mosaic animals) of KO-*JHAMT*, *CYP15A1*, *Met*, or *Kr-h1* exhibited high mortality during late embryogenesis, indicating that JH is necessary for the differentiation and maturation of embryonic tissues in ametabolous insects. Whole embryo transcriptomes revealed that the highest expressions of the JH signaling gene, *Kr-h1*, coincided during late embryogenesis. Using embryonic legs as an example, we employed comparative transcriptome analysis to explore the molecular mechanism by which JH signaling promotes tissue maturation during embryonic development in *T. domestica*. In addition, our comparative studies demonstrated similar embryonic actions of JH on the hemimetabolous insect *G. bimaculatus*. Ultimately, we speculated that the postembryonic anti-metamorphic functions of JH originated from the primitively embryonic role during the evolution of insect metamorphosis.

Results

JH signaling is high during late embryogenesis in *T. domestica*

To investigate the potential role of JH signaling during embryogenesis of *T. domestica*, we initially elucidated the embryonic development pattern and established a detailed morphological description of the embryo using scanning electron microscopy (SEM) and DAPI staining. As shown in Fig. 1A–F, T. *domestica* follows a typical

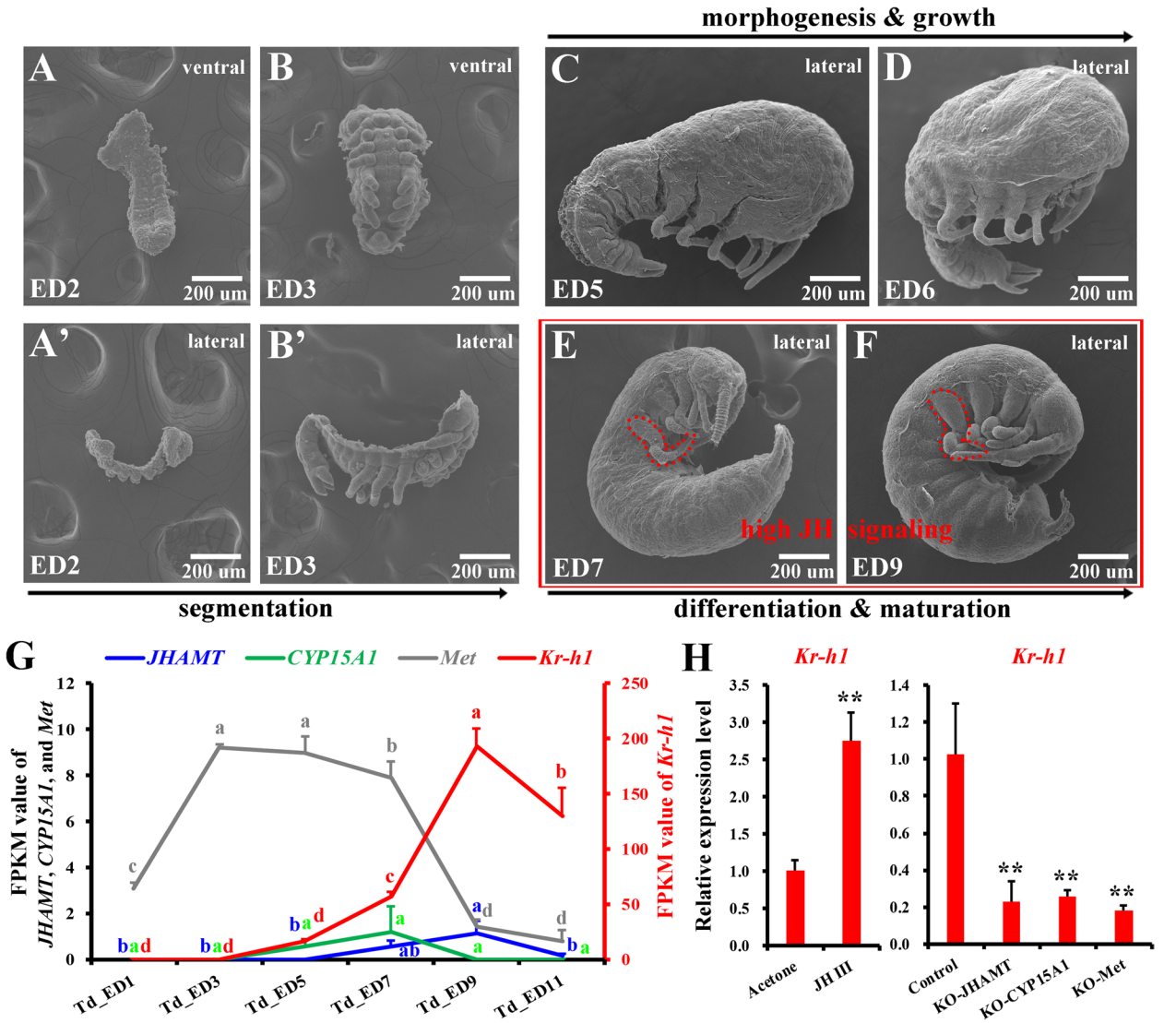

Fig. 1 Correlation between the morphological changes of embryo and JH signaling in *T. domestica*. **A**–**F** Morphological pattern of embryo during embryonic development in *T. domestica*, as observed through scanning electron microscopy (SEM). Ventral (**A**) and lateral (**A'**) views of the newly formed germ band containing only the most anterior cephalic and thoracic segments at day 2 after egg laying (ED2). Ventral (**B**) and lateral (**B'**) views of the germ band with completed segmentation observed at ED3. Dorsal closure, progressing from posterior to anterior, initiates at ED5 (**C**), advances at ED6 (**D**), and concludes at ED7 (**E**). By ED7, morphogenesis and segmentation of the legs are completed, followed by differentiation and maturation of tissues and organs, including legs, until hatching. The shedding of the first embryonic (E1) cuticle occurs at ED9 (**F**). **G** Transcriptional dynamics of key genes involved in JH biosynthesis and signaling in whole eggs of *T. domestica*. FPKM (Fragments Per Kilobase of exon model per Million mapped fragments, which indicates gene expression level in RNA-seq) values of *JHAMT*, *CYP15A1*, *Met*, and *Kr-h1* were obtained from RNA-seq data generated from wild-type eggs collected at ED1, ED3, ED5, ED7.ED9, and ED11, respectively. **H** Effect of JH III application and knockout (KO) of *JHAMT*, *CYP15A1*, and *Met* on *Kr-h1* expression in whole eggs of *T. domestica*. Relative expression levels of *Kr-h1* were detected using qPCR, with the ribosomal protein S26 (*RPS26*) as the reference gene. JH III (100 ng/egg) was applied at ED6, and treated eggs were collected 12 h post-treatment for qPCR analysis (the acetone treated eggs as controls). Gene-specific gRNAs (400 ng/μL) and Cas9 (300 ng/μL) were injected into the freshly laid eggs within 3 h, and eggs were collected at ED10 for qPCR analysis (the eggs injected with Cas9 as controls). All RNA-seq and qPCR data are presented as the mean ± s.e.m. ($n = 3$)

short-germ band type of embryonic development (also see Additional file 1: Fig. S1), wherein only the most anterior cephalic and thoracic segments of the embryo are specified during the early syncytial blastoderm stage (embryonic day 2, ED2; A and A'). The abdominal segments are subsequently added in sequence from a posteriorly located undifferentiated growth zone (GZ) during germ band elongation (B, B'). From germ band formation

(ED3), morphogenesis of the tissues and organs of each embryonic layer takes place, with the germ band giving rise to a fully segmented embryo by ED7 when dorsal closure ends (C–E). Morphogenetic growth and segmentation of the legs occur simultaneously. Differentiation and maturation occur from ED7, during which embryonic legs become plump and stout when viewed from the outside (E, F). After completing embryogenesis, the embryo hatches as the first instar juvenile during ED11–12. Our study is consistent with a recent observation (Truman et al., [39]).

Next, we examined the expression levels of genes involved in JH biosynthesis and signaling during embryonic development in *T. domestica* using RNA-seq to establish a correlation between the morphological changes of the embryo and the presence of JH signaling. *T. domestica*already possesses the ability to produce JH III [9]. The transcripts of*JHAMT* and *CYP15A1* remained low (FPKM < 3) throughout the entire period of embryogenesis, with small peaks observed at ED9 and ED7, respectively. The mRNA abundance of *Met* was relatively high during the morphogenesis and growth period (ED3–ED7), while the expression level of *Kr-h1* was massively upregulated from ED7 onward and remained high during differentiation and maturation period (ED7–ED11) (Fig. 1G).

We further investigated whether the JH signaling pathway known in metamorphic insects had already existed during embryonic development in ametabolous firebrats. *Kr-h1* gene expression was significantly upregulated in the embryos of *T. domestic*a after JH III treatment at ED6 compared with the acetone treated control. Conversely, CRISPR/Cas9-meditated gene knockout (KO) of *JHAMT*, *CYP15A1*, and *Met* respectively resulted in downregulation of *Kr-h1* transcription level at ED10 in the mosaic mutants of G0 (generation 0) once compared with that in the controls (Fig. 1H).

Collectively, the JH signaling pathway primitively exists in embryogenesis of ametabolous insects, and JH signaling is highly activated during late embryogenesis, suggesting that JH signaling is functionally important for embryonic differentiation and maturation in ametabolous insects.

JH signaling-deficient embryos exhibit wrinkled and feeble legs in *T. domestica*

Subsequently, we examined the embryonic phenotypes of JH-deficient (KO-*JHAMT*, KO-*CYP15A1*) and JH signaling-deficient (KO-*Met*, KO-*Kr-h1*) mutants; genomic DNA modifications were confirmed via Sanger sequencing (Additional file 1: Fig. S2A–D). We observed a significant reduction in embryo hatchability (Fig. 2A); however, the timing of hatching was not delayed in the remaining G0 mosaic mutants of *JHAMT*, *CYP15A1*, *Met*, or *Kr-h1* compared to the control population (Fig. 2B). These findings indicate that the absence of JH or JH signaling results in significant lethality in embryos of the ametabolous *T. domestica*. We dissected the eggshells to observe the developmental progress of the unhatched mutant embryos on embryonic day 14 (ED14). The phenotypes observed in the unhatched eggs were classified into four classes (refer to Additional file 1: Fig. S3): class I (embryos displaying apparent completion of embryogenesis without extraembryonic fluid); class II (embryos that had completed dorsal closure but failed to resorb their extraembryonic fluid); class III (embryos that had not completed dorsal closure, characterized by "big heads"); class IV (cloudy liquid devoid of embryos, including the absence of germ bands). The statistical analysis results showed that class II comprise of the highest proportion, followed by class I, in the embryos of KO-*JHAMT*, *CYP15A1*, *Met*, and *Kr-h1* G0 mutants, respectively (refer to Fig. 2C). Preliminary phenotype examinations suggest that JH signaling plays a crucial role in the resorption of extraembryonic fluid and hatching during late embryogenesis in ametabolous insects.

Furthermore, we conducted SEM examinations to investigate the specific external phenotypes of the mutant embryos classified as class II and class I at ED14. Under a light microscope, control embryos exhibited a white body with elongated and robust appendages (Fig. 2D). However, in class II embryos of KO-*JHAMT*, *CYP15A1*, *Met*, and *Kr-h1* G0 mutants, which appeared yellowish, unabsorbed extraembryonic fluid adhered to the body, resulting in appendages such as legs becoming stuck (Fig. 2E–H). SEM results showed that the class II mutant embryos displayed shrunken and feeble legs when compared to those of control embryos (Fig. 2D'–H'). A small portion of class II embryos displayed even more pronounced morphological abnormalities than previously described: body structures were difficult to discern, and the legs were notably shrunken (Additional file 1: Fig. S4A–E_1'). Mutant embryos at class I displayed a dry body surface with stretched-out but wrinkled legs (see Additional file 1: Fig. S4A–E_2'). Collectively, the morphological defects observed in CRISPR/Cas9-mediated KO-*JHAMT*, *CYP15A1*, *Met*, and *Kr-h1* indicate the indispensable role of JH signaling in leg maturation during late embryogenesis in ametabolous insects.

JH promotes leg maturation by inducing energy supply and muscle development

We conducted RNA-seq experiments to further explore the molecular mechanisms underlying JH-dependent leg maturation during embryogenesis in *T. domestica*. Embryonic legs were dissected from control specimens,

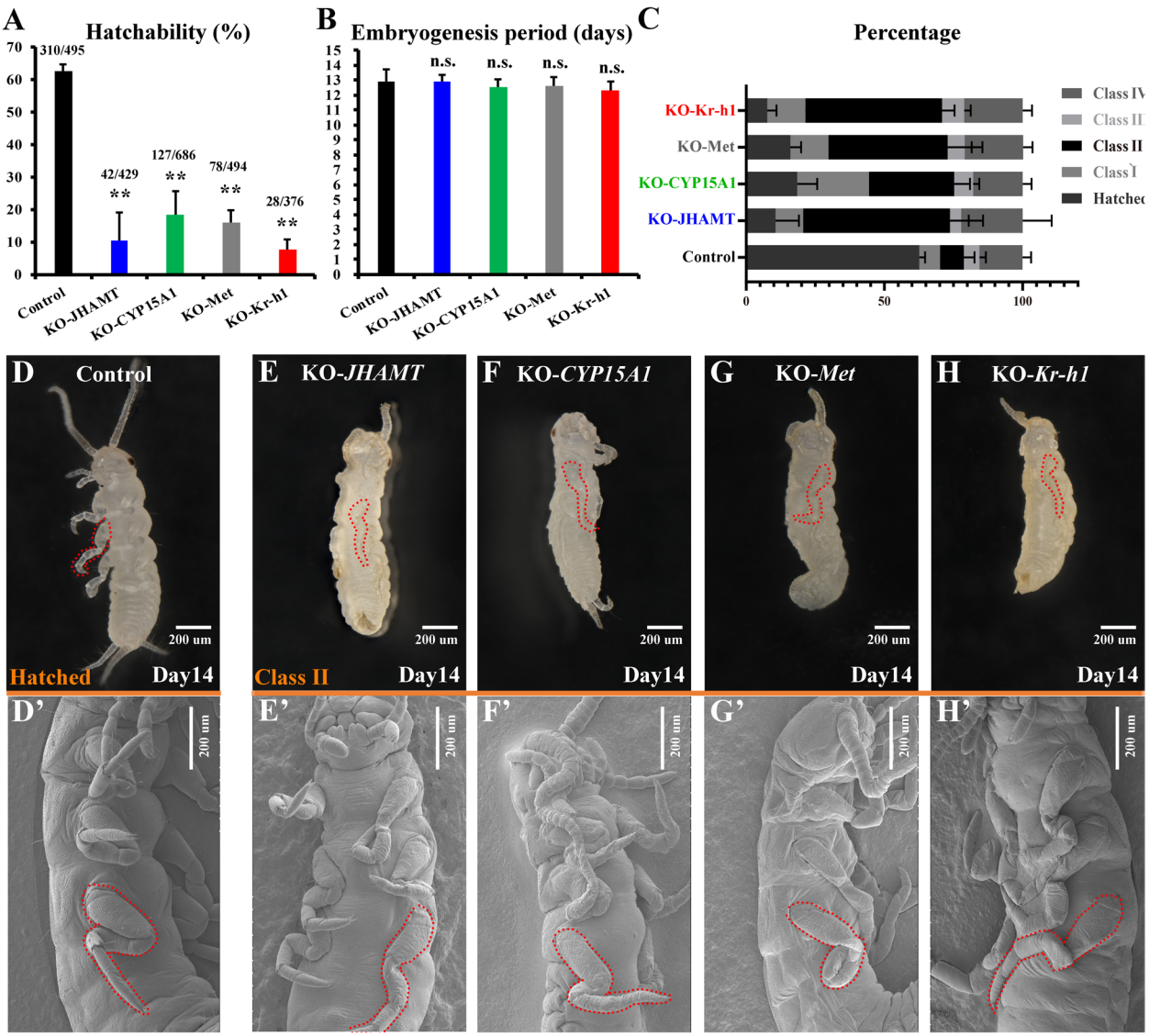

Fig. 2 Effects of JH signaling deprivation on embryogenesis of *T. domestica*. Hatchability (**A**) and embryogenesis period (**B**) by the G0 mosaic mutants (including KO-*JHAMT*, KO-*CYP15A1*, KO-*Met*, and KO-*Kr-h1*). Hatched juveniles were counted at ED14, and the numbers above bars indicate the number of hatched/total embryos. The embryogenesis period was recorded at 12-h interval. **C** Phenotypes of unhatched embryos counted at ED14 according to classification grades (see Additional file 1: Fig. S3). Bars indicate mean ± s.e.m. for percentage (**A**, **C**, $n = 4$ or 5 batches) or days of embryogenesis (**B**, $n = 310$ individuals for control; 42 for KO-*JHAMT*; 127 for KO-*CYP15A1*; 74 for KO-*Met*; 28 for KO-*Kr-h1*) for each population. **D**–**H'** Embryo phenotypes resulting from KO-*JHAMT*, KO-*CYP15A1*, KO-*Met*, and KO-*Kr-h1* in *T. domestica*. Photos collected by optical microscope (**D**–**H**) and scanning electron microscopy (SEM) (scale bar = 200 μm) (**D'**–**H'**) are shown. **D**, **D'** Normal freshly eclosed first instar juvenile. Class II embryos of *JHAMT* (**E**, **E'**), *CYP15A1* (**F**, **F'**), *Met* (**G**, **G'**), and *Kr-h1* (**H**, **H'**) G0 mutants. The legs were highlighted by red dashed lines

as well as KO-*JHAMT*, *CYP15A1*, *Met*, and *Kr-h1* G0 mutants, at both ED10 and ED11 (mixed in a ratio of 6:4) for RNA-seq analysis. Through four sets of comparative transcriptome analyses, we identified differential expression patterns, with 2414 downregulated and 2722 upregulated genes in KO-*JHAMT* vs. control, 2160 downregulated and 2542 upregulated genes in KO-*CYP15A1* vs. control, 2166 downregulated and 2358 upregulated genes in KO-*Met* vs. control, and 2576 downregulated and 2325 upregulated genes in KO-*Kr-h1* vs. control individuals. Notably, mutations in *JHAMT*, *CYP15A1*, and *Met* both resulted in significant downregulation of *Kr-h1* expression level in the legs (Fig. 3A, C, E, G). KEGG enrichment analysis revealed a high consistency in significantly downregulated pathways across all four comparative analysis mentioned above (the top 15 pathways

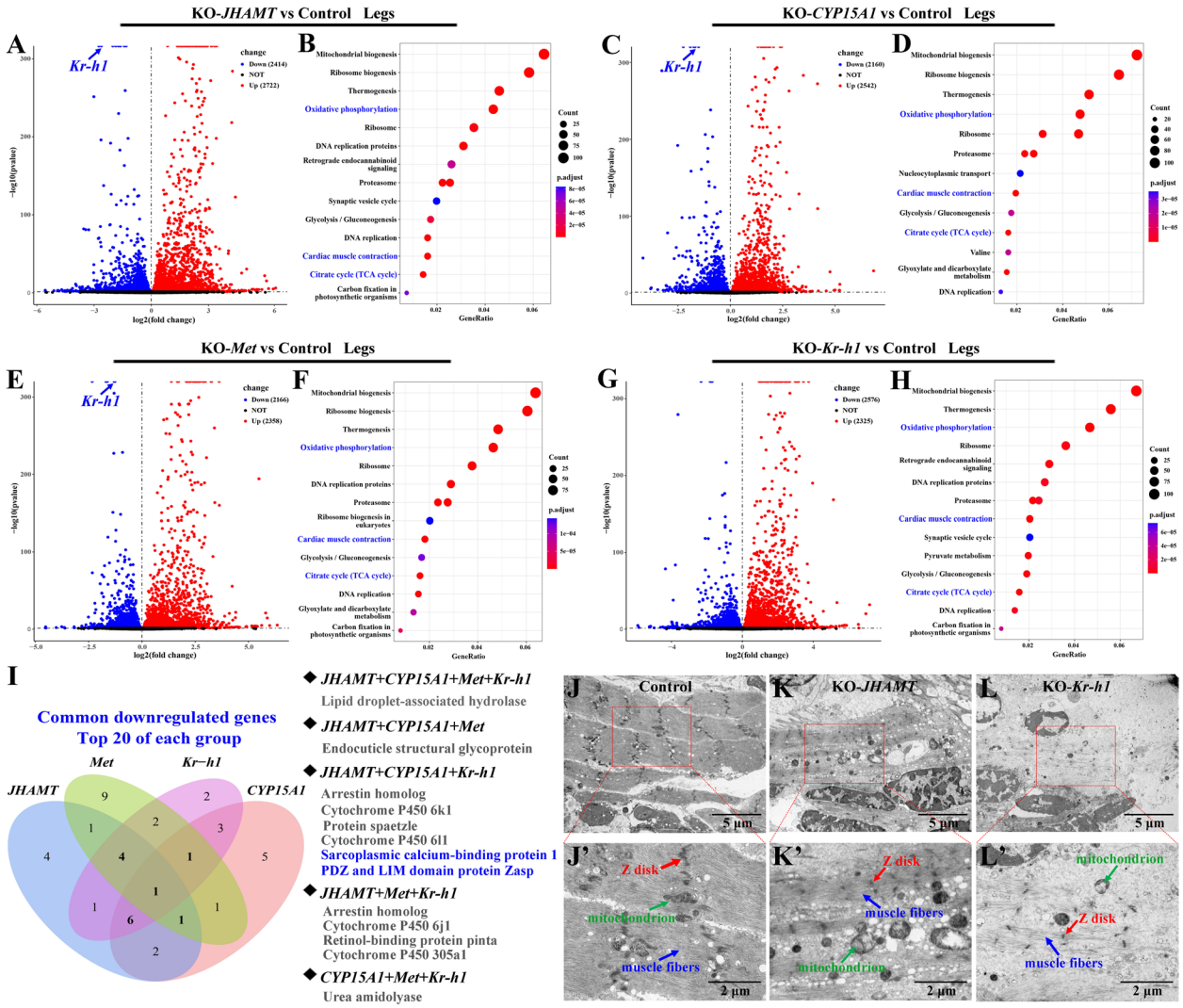

Fig. 3 Effects of JH signaling deprivation on the transcriptional profiles in embryonic legs of *T. domestica*. Volcano plots (**A**, **C**, **E**, **G**) and KEGG enrichment bubble maps (**B**, **D**, **F**, **H**; top 15 downregulated pathways) are generated from comparative analysis of embryonic leg transcriptomes in *T. domestica*. The embryonic legs were sampled at ED10 and ED11 (mixed in a ratio of 6:4) from control, KO-*JHAMT*, KO-*CYP15A1*, KO-*Met*, and KO-*Kr-h1* embryos of G0 for RNA-seq. Differential expression analyses were conducted according to the schemes of KO-*JHAMT* vs. control (**A**, **B**), KO-*CYP15A1* vs. control (**C**, **D**), KO-*Met* vs. control (**E**, **F**), and KO-*Kr-h1* vs. control (**G**, **H**), respectively; genes with an adjusted *P* value < 0.05 (with no threshold for fold change) are designated as differentially expressed. Each group contained three independent biological replicates, and at least 200 embryos classified as class II or class I were pooled to generate one biological replicate. CRISPR/Cas9-mediated knockout of JH biosynthesis genes (*JHAMT*, *CYP15A1*) or JH receptor genes (*Met*) significantly suppressed JH signaling, as indicated by the expression level of *Kr-h1* on the volcano plots. Oxidative phosphorylation, TCA cycle, and muscle contraction pathways are highlighted in blue on the bubble maps. I Venn diagram analysis of commonly downregulated, top 20 (fold change) annotated genes from the four groups of comparative transcriptomes. Genes that simultaneously appeared within at least three groups are listed, with two muscle activity-related genes, sarcoplasmic calcium-binding protein 1 and PDZ and LIM domain protein Zasp, highlighted in blue. Histological changes of the leg muscles from control (**J**), KO-*JHAMT* (**K**), and KO-*Kr-h1* (**L**) embryos at ED11, as observed through transmission electron microscopy (TEM). Detailed magnifications of muscle fibers in **J**–**L** (red boxes) are shown in **J'**–**L'**. The Z-disks, muscle fibers, and mitochondria were indicated with the red, blue, and green arrows, respectively

are listed in Fig. 3B, D, F, H), including those associated with energy supply (such as mitochondrial biogenesis, thermogenesis, oxidative phosphorylation, the TCA (tricarboxylic acid) cycle, and glycolysis/gluconeogenesis), muscle contraction, as well as some protein synthesis and degradation pathways (including ribosome biogenesis, ribosome function, and proteasome activity). In addition, pathways related to neural signal transduction, such as retrograde endocannabinoid signaling and the synaptic vesicle cycle, showed significant downregulation in

embryonic legs upon suppression of JH signaling. Notably, these two neural signal transduction pathways were not included among the top 15 downregulated pathways in the KO-*CYP15A1* vs. control and KO-*Met* vs. control groups (refer to Additional file 1: Tables S1–4 for a complete list of significantly downregulated pathways, with adjusted P values < 0.05). Similarly, the phenotype analysis revealed that there were more severe developmental defects in the KO-*JHAMT* or KO-*Kr-h1* G0 mutants compared to KO-*CYP15A1* or KO-*Met* (Fig. 2C). Similarly, the significantly upregulated pathways identified through KEGG analysis showed high consistency (refer to Additional file 1: Fig. S5A–D).

Additionally, we conducted Venn analysis on the four sets of significantly downregulated genes, revealing 1195 genes that are commonly downregulated among all four groups (Additional file 1: Fig. S6A). Subsequently, the top 20 annotated genes, sorted by fold change in ascending order, from each group were extracted from the commonly downregulated gene set (Additional file 1: Fig. S6B), and these genes were then subjected to another Venn analysis (Fig. 3I). The genes that appeared simultaneously in three or four groups were listed in the figure: lipid droplet associated hydrolase, urea amide hydrolase, and cytochrome P450 genes involved in energy supply and material metabolism; spaetzle involved in immunity; arrestin homolog involved in GPCR signaling; retinol binding protein involved in retinoic acid signaling; sarcoplasmic calcium binding protein and PDZ and LIM domain protein Zasp associated with muscle structure and contraction. Both of the aforementioned analysis schemes highlighted the importance of muscle development and activity. Examination of the leg muscles via transmission electron microscopy (TEM) at ED11 showed that both KO-*JHAMT* and KO-*Kr-h1* severely halted the progression of muscle fiber development, specifically, there were abundant and integrated muscle fibers between Z-disks in the legs of control animals, however, the two mutant specimens exhibited obvious deficiencies of the muscle fibers between Z-disks, thereby hindering leg maturation compared to the control (Fig. 3J–L'). In summary, the transcriptome and TEM results collectively indicate that JH signaling plays a pivotal role in energy supply and muscle development in the legs during the late embryogenesis in *T. domestica*.

JH signaling promotes embryonic leg maturation in *G. bimaculatus*

Next, we aimed to determine whether the fundamental role of JH signaling observed in the embryonic legs of *T. domestica* extends to hemimetabolous insects, which evolved from ametabolous ancestors. To address this, we employed *G. bimaculatus* as a model representative of hemimetabolous insects. The embryogenesis of *G. bimaculatus* lasts approximately 11–12 days, showing a good correspondence in the pattern of embryonic development timing compared to *T. domestica*. Similarly, germ band formation and dorsal closure are completed by ED3 and ED7 in *G. bimaculatus*, respectively. Subsequently, differentiation and maturation occur from ED7 until hatching [15]. The investigation into the expression patterns of *JHAMT*, *CYP15A1*, *Met*, and *Kr-h1* during embryonic development in *G. bimaculatus*, using RNA-seq, revealed that all four genes exhibit expression peaks during differentiation and maturation period (Fig. 4A). By using CRISPR/Cas9-mediated genome editing, we conducted *Kr-h1* loss-of-function experiments in *G. bimaculatus* (Additional file 1: Fig. S2E) to evaluate the potential roles of JH signaling in regulating embryonic development in hemimetabolous insects. The *Kr-h1* G0 mutants of *G. bimaculatus* were unable to hatch, with the majority (~ 60%) arrested at class I (Fig. 4B, counted at ED13), similar to observations in *T. domestica*. The unhatched embryos exhibited swollen (femur) and twisted (tibia) legs, particularly the jumping legs on the third thoracic segment. Additionally, they showed cuticle tanning within eggshells (Fig. 4B', B").

Comparative transcriptome experiments were also utilized to explore the molecular mechanisms by which JH regulates embryonic leg maturation in *G. bimaculatus*. Embryonic legs dissected at ED10 and ED11 (mixed in a 6:4 ratio) from KO-*Kr-h1* and control embryos were subjected to RNA-seq. Notably, among the 2159 downregulated genes in *G. bimaculatus*, 4 of them, including lipid droplet-associated hydrolase, cytochrome P450 6k1, cytochrome P450 6j1, and PDZ and LIM domain protein Zasp, were also among the 13 genes screened through Venn analysis in *T. domestica* (Fig. 4C, related to Fig. 3I); the top 15 pathways included energy supply pathways (thermogenesis, oxidative phosphorylation, and TCA cycle), cardiac muscle contraction, and the neural transduction related retrograde endocannabinoid signaling, mirroring pathways identified in *T. domestica*. In addition, other pathways involved in muscle development and activity were significantly downregulated in the embryonic legs of *G. bimaculatus* when JH signaling was inhibited, compared to the control, including adrenergic signaling in cardiomyocytes, the cGMP-PKG signaling pathway, vascular muscle contraction, and the calcium signaling pathway (Fig. 4D; Additional file 1: Fig. S7A, Table S5). However, the pathways that showed upregulation in the embryonic legs between the two species exhibited inconsistency when JH signaling was blocked (Additional file 1: Fig. S7A, B; Fig. S5). Since muscles are an important component of the legs, we further investigated the downregulated genes within the cardiac muscle

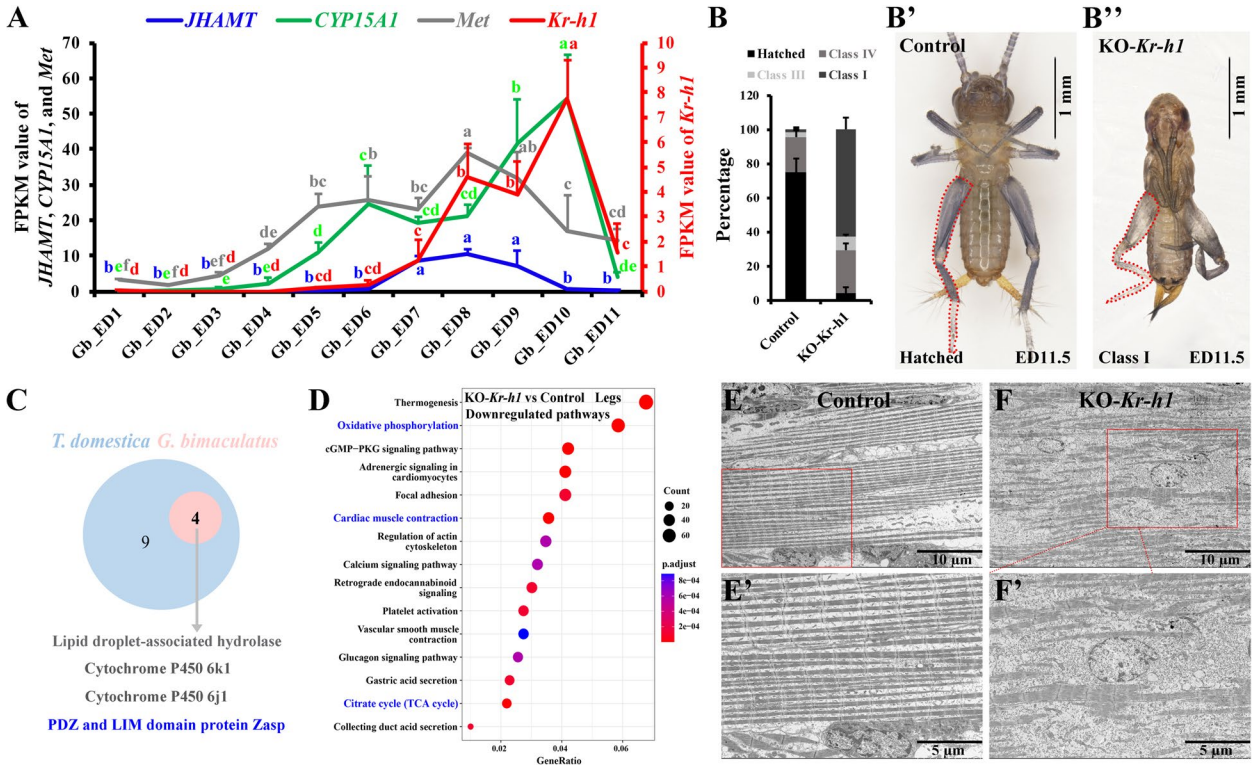

Fig. 4 JH signaling is essential for leg maturation in embryos of *G. bimaculatus*. **A** Expression of *JHAMT*, *CYP15A1*, *Met*, and *Kr-h1* in embryos of *G. bimaculatus*. The FPKM values in whole eggs at different ages from ED0 to ED11 are presented. RNA-seq data are represented as the mean ± s.e.m. for three biological replicates. **B**–**B″** Embryo phenotypes resulting from CRISPR/Cas9-mediated knockout of *Kr-h1* (G0 mutants) in *G. bimaculatus*. Statistical analysis of the embryos of control and KO-*Kr-h1* on ED13 (G0, $n = 3$ batches) is shown in **B**, following the classification criteria in *T. domestica*. Phenotype observation of the control (**B**, hatched) and KO-*Kr-h1* (**B′**, class I) embryo at ED11.5. The legs were highlighted by red dashed lines. **C** Four genes, which are included in the gene set (screened through Venn analysis in *T. domestica*, containing 13 genes, refer to Fig. 3I), were also significantly downregulated in the embryonic legs of *Kr-h1* G0 mutants in *G. bimaculatus* compared with those in control (transcriptome data). PDZ and LIM domain protein Zasp is highlighted in blue. **D** KEGG bubble map (top 15 downregulated pathways) derived from comparative transcriptomes (KO-*Kr-h1* vs. control) of embryonic legs in *G. bimaculatus*. Embryonic legs were collected at ED10 and ED11 (mixed in a ratio of 6:4) from control and G0 mutants for RNA-seq. Genes with an adjusted *P* value < 0.05 (with no threshold for fold change) are considered differentially expressed. Each group contained three independent biological replicates, and at least 200 embryos classified as class I were pooled to generate one biological replicate. Oxidative phosphorylation, TCA cycle, and muscle contraction pathways are highlighted in blue on the diagram. **E**, **F** TEM observation of leg muscles in control and KO-*Kr-h1* embryos at ED11. Detailed magnifications of muscle fibers in **E** and **F** (red boxes) are shown in **E′** and **F′**, respectively

contraction pathway enriched in both *T. domestica* and *G. bimaculatus.* We discovered 12 genes that were consistently downregulated in both species, including calcium transport proteins such as voltage-dependent L-type Ca^{2+} channel, Na^{+}/Ca^{2+} exchanger, and sarco/endoplasmic reticulum Ca^{2+}-ATPase, as well as muscle structural proteins like tropomyosin and myosin heavy chain, alongside certain respiratory chain complex proteins (Additional file 1: Fig. S7C). Examination of the leg muscles using TEM showed that the 11-day-old control embryos displayed intact muscle fibers, whereas the KO-*Kr-h1* embryos exhibited obvious defects in their muscle fibers (Fig. 4E–F'). These findings suggest that JH signaling plays a conserved role in promoting embryonic leg maturation across both ametabolous and hemimetabolous insects.

Discussion

JH signaling is indispensable for late embryogenesis in ametabolous and hemimetabolous insects

While JH treatment has been shown to promote growth/differentiation switch in ametabolan and hemimetabolan embryos [38, 39], the specific molecular mechanisms of its actions during the embryonic period remain relatively unexplored. In this study, we aimed to provide genetic evidence supporting the role of JH signaling during embryonic development. We employed CRISPR/Cas9-mediated gene knockout techniques to genetically

deprive JH or JH signaling, using*T. domestica* (firebrat, ametabolan) and *G. bimaculatus* (cricket, hemimetabolan) as model organisms for our evo-devo studies. Analyses of embryonic development patterns and gene expression profiles suggest that high levels of JH signaling emerge in late embryogenesis, coinciding with the embryo's terminal differentiation stage in both species (Figs. 1, 4). Knockout firebrats reveal an indispensable role for JH signaling in terminal maturation and hatching during embryogenesis (Fig. 2), consistent with the effects of blocking JH production via treatment with 7-ethoxyprecocene (7EP) [39]. Similarly, knockout crickets demonstrate a similar role of JH signaling in embryonic development (Fig. 4), with the legs of the unhatched embryos showing a distinct impediment in terminal differentiation and maturation (appearing wrinkled, feeble, or twisted) after JH signaling deprivation. Hence, embryonic legs were chosen as a model to explore the molecular mechanisms underlying JH-dependent tissue maturation during the embryogenesis of ametabolous and hemimetabolous insects, utilizing RNA sequencing.

A significant advancement in our study is the further exploration of the mechanisms of JH actions during embryogenesis of insects. Comparative transcriptome experiments reveal that JH promotes the differentiation and maturation of embryonic legs by activating genes responsible for energy metabolism, Ca^{2+}-dependent muscle contraction, and neural signal transduction in both *T. domestica* and *G. bimaculatus* (Figs. 3, 4), indicating the molecular mechanisms of JH function in the late embryogenesis are conserved between ametabolous and hemimetabolous insects. We hypothesize that JH signaling maintains energy supply to ensure the development and maturation of muscles and nerves. Speculatively, the transcriptional regulation of JH-dependent metabolic homeostasis and energy supply may have been redeployed during postembryonic life, playing a crucial role in controlling metamorphosis, reproduction, and polyphenism [4, 19, 36, 41]. In addition, JH-dependent Ca^{2+}-homeostasis represents another well-conserved mechanism of JH action that may have been extended into postembryonic development [14, 24, 27, 28, 43]. We are inclined to support the hypothesis that the ancestral functions of JH in insects were primarily confined to embryogenesis [39]. However, in the current study, we did not rule out a role of JH in reproduction of the ametabolous insect. Therefore, studying the molecular mechanisms of JH actions in various developmental events of diverse insect groups would provide a better understanding of the ancestral roles of JH and how JH signaling has acquired anti-metamorphic actions as well as other pleiotropic actions during the evolution of insects.

Modifications in embryonic JH function during evolution of insect metamorphosis

The evolution of insects was accompanied by profound changes in their life histories. One significant change involved modifications to postembryonic growth, which facilitated the evolution of wings and power flight. These modifications led to the emergence of a hemimetabolous lifestyle. Hemimetabolan species hatch as nymphs, which are morphologically similar to the adults. The subsequent step to holometabolous evolution involved a redirection of embryogenesis so that the insect hatching from the egg emerged as a modified larva. The transition from larva to adult then occurred through an intermediary stage known as the pupa [7, 20, 38].

Extensive differences in the roles of JH during embryogenesis have been demonstrated between holometabolous and ametabolous/hemimetabolous insects [20, 38]. Truman and Riddiford [37, 38] equated the larva–pupa–adult of the Holometabola to the pronymph (a cryptic embryonic stage)–nymph–adult stages of hemimetabolous insects. According to their pronymph theory, the larval form arose through "de-embryonization," wherein ancestral programs of embryonic development were arrested. This concept is elegantly explained by the discontinuous development of the central nervous system, eye, and leg of holometabolous larvae. Specifically, in ametabolous and hemimetabolous groups, the newly hatched juvenile/nymph already possess fully functional legs similar to the adult form, following differentiated growth and maturation during embryogenesis (pronymph). However, in embryos of holometabolous species, they initially develop intermediate legs adapted to larval needs and may even produce legless larvae. Subsequently, the differentiation of larval legs or leg primordia resumes during larval or pupal stage. Therefore, the embryonic JH function, which promotes terminal differentiation and maturation, had been speculatively arrested and postponed, thus appeared inessential during embryogenesis of holometabolous insects.

Despite genetic interruption of the JH signaling having little effect on embryogenesis in the holometabolous species, JH (peak) signaling is indeed present during the middle to late stages of embryonic development, as observed in holometabolous species such as *Bombyx mori* [13] and *Drosophila melanogaster* [10]. Moreover, recent reports have highlighted additional roles of JH signaling, such as directing primordial germ cell migration to the embryonic gonad [6]. Consequently, there is an urgent need to uncover more hidden functions of embryonic JH in insects to further delineate the trajectories of the functional evolution of JH signaling.

Conclusions

JH serves as the primary endocrine hormone involved in maintaining the juvenile stages and preventing metamorphosis in insects. The development of embryos determines the type of juveniles and the subsequent nature of metamorphosis. While the role of JH signaling in regulating metamorphosis is well-characterized, its function during embryonic development remains poorly understood. Our study contributes genetic evidence supporting the role of JH signaling in promoting tissue differentiation and maturation during embryonic development in both ametabolous and hemimetabolous insects. Furthermore, by using embryonic legs as an example, we elucidate the molecular mechanisms by which JH signaling promotes tissue maturation during late embryogenesis. This study sheds light on the functional evolution of JH throughout the evolutionary journey of insect metamorphosis.

Methods

Insects

The firebrats, *T. domestica*, were reared in the dark at 37 ± 0.5 °C and 70–80% relative humidity in plastic containers and were fed commercial rat food. The crickets, *G. bimaculatus*, were kept at 28 °C with a relative humidity of 60%, under a 12:12-h light/dark photoperiod, in plastic boxes, and were fed commercial fish feed and tap water. Eggs of both species were collected from absorbent cotton at 12-h intervals and subsequently incubated until reaching the designed time points for RNA-seq analysis.

JH III application

For hormone treatments, JH III (Cayman, USA) was dissolved in acetone to prepare a working solution of 1 mg/mL. This solution was applied to the eggs of *T. domestica* (100 nL/egg) at ED6 using a NanoInject II microinjector (Drummond Scientific, USA). The same volume of acetone was applied as a control.

Scanning electron microscopy (SEM)

For SEM analysis, the embryos were initially fixed in a solution containing 2% paraformaldehyde and 2.5% glutaraldehyde at 4 °C overnight. Subsequently, they were rinsed with 0.1 mol/L phosphate buffer (pH = 7.2) and postfixed with 1% osmic acid at room temperature for 2 h. Afterward, the specimens underwent dehydrated in ethanol, followed by gradual transfer to acetone. Finally, they were dried using a critical point dryer (Leica EM300). The dried specimens were then mounted onto sample stage using double-sided carbon tape, coated with a thin layer of gold, and observed under a scanning electron microscope.

Transmission electron microscope (TEM)

Newly collected legs at ED11 were first fixed in 2.5% glutaraldehyde at 4 °C overnight, followed by thorough washing with PBS. The specimens were then postfixed in 0.5% osmium tetroxide for 2 h. Next, they were dehydrated in an ethanol gradient and finally embedded in Epon resin. Longitudinal Sects. (70 nm) of muscle fibers were prepared using a UC7 ultramicrotome (Leica). These sections were then stained with Reynolds' lead citrate and visualized using an HT7700 transmission electron microscope (Hitachi, Tokyo, Japan) to observe the degree of breakage of muscle fibers and the morphology of mitochondria.

CRISPR/Cas9-mediated gene knockout

The 20 bp sgRNA targets immediately upstream of the PAM site were designed using the software sgRNAcas9 [40]. Gene-specific sgRNAs (two gRNAs targeting one gene) were then transcribed in vitro from synthesized DNA templates and column-purified using a GeneArt™ Precision gRNA synthesis kit (Invitrogen, USA) following the manufacturer's instructions. The primers used for gRNA biosynthesis are listed in Additional file 1: Table S6. Synthesized sgRNAs were stored at − 80 °C until use. Fertilized eggs were collected within 3 h after oviposition and aligned on double-sided tape on a glass slide. Microinjections were performed using a FemtoJet 4r micromanipulator coordinated with a FemtoJet 4i microinjector (Eppendorf, Germany), under an SZX16 microscope (Olympus, Japan). In *T. domestica*, the final concentration of each gRNA was 400 ng/μL, and that of Cas9 was 300 ng/μL [5]. In *G. bimaculatus*, the final concentration of each gRNA was 800 ng/μL, and that of Cas9 was 500 ng/μL. The control eggs were only injected with Cas9 at the same dosage. The solution was injected into the eggs with glass capillary tubes (Drummond Scientific, USA). Injected eggs were incubated in the corresponding rearing environment, respectively, for subsequent experiments. The G0 individuals were genotyped by PCR product sequencing using primers designed to detect mutagenesis around the gRNA target sites of the target gene. The specific primers are shown in Additional file 1: Table S7.

Quantitative real-time PCR (qPCR)

qPCR was employed to detect the *Kr-h1* expression levels in embryos after JH III application or following the knockout of selected genes by sgRNA injection. Whole eggs (at least 30 eggs were pooled for one sample) were collected at 12 h after JH III treatment or at ED10 after

sgRNA injection for qPCR analysis. Total RNA was extracted from the embryos utilizing AG RNAex Pro reagent (Accurate Biology, China) according to the manufacturer's protocol. cDNA was synthesized with reverse transcriptase M-MLV (Vazyme, China) following the manufacturer's instructions. qPCR was performed using SYBR® Select Master Mix (Yeasen, China) and the Applied Biosystems QuantStudio™ 6 Flex Real-Time PCR System (Thermo Scientific, Waltham, MA, USA). The ribosomal protein S26 (*RPS26*) was chosen as a reference gene for relative expression analysis [3]. The primers used for qPCR analysis are listed in Additional file 1: Table S8.

RNA-seq and data analysis

The databases of temporal gene expression profiles in whole embryos (two species, *T. domestica* and *G. bimaculatus*) were established through RNA-seq, with at least 30 eggs per sample prepared for RNA extraction. Additionally, the embryonic legs of firebrats and crickets from both G0 mutant and wild-type control groups were collected (with more than 200 individuals per sample) at ED10 and ED11 (mixed in a ratio of 6:4) for RNA-seq analysis, aimed at elucidating the transcriptional regulatory mechanism. Each group comprised three independent biological replicates. Total RNA was prepared from the target tissues using Trizol reagent. Library construction, sequencing using an Illumina NovaSeq 6000, and mapping to the genomes with the Genomic Short-read Nucleotide Alignment Program (GSNAP) were carried out by BMKGENE (Beijing, China). A whole genome of *T. domestica* was establish in our laboratory. The reference genome of *G. bimaculatus*were obtained from the NCBI database [44], https://www.ncbi.nlm.nih.gov/datasets/genome/GCA_017312745.1/). Gene expression levels were estimated by fragments per kilobase of transcript per million fragments mapped (FPKM). Differential expression analysis between two groups was conducted utilizing the DESeq R package (1.10.1). Genes with an adjusted *P* value (false discovery rate, FDR) < 0.05, as determined by DESeq, were considered differentially expressed. We utilized KOBAS software to evaluate the statistical enrichment of differentially expressed genes in KEGG pathways.

Data analyses and statistics

Statistical analyses were performed with Student's *t*-test or ANOVA using IBM SPSS Statistics 19.0 software. A two-tailed, unpaired Student's *t*-test was used to compare differences between two groups at the same time point (***P* < 0.01, n.s., not significant). For ANOVA, different letters indicate statistically significant differences between multiple groups using the LSD method (*P* < 0.05).

Abbreviations

JH	Juvenile hormone
CRISPR/Cas9	Clustered Regularly Interspaced Short Palindromic Repeats/CRISPR-associated protein 9
KO	Knockout
JHAMT	Juvenile hormone acid methyltransferase
CYP15A1	Methyl farnesoate epoxidase
Met	Methoprene-tolerant
Kr-h1	Krüppel homolog 1
TEM	Transmission electron microscopy
RNAi	RNA interference
Evo-devo	Evolutionary developmental biology
G0	Generation 0
SEM	Scanning electron microscopy
DAPI	4′,6-Diamidino-2-phenylindole
ED	Embryonic day
GZ	Growth zone
RNA-seq	RNA sequencing
FPKM	Fragments Per Kilobase of exon model per Million mapped fragments
KEGG	Kyoto Encyclopedia of Genes and Genomes
TCA	Tricarboxylic acid
GPCR	G protein-coupled receptor
PDZ	PSD-95/discs-large/zonula occludens-1
LIM	Lin-Isl-Mec
ZASP	ZO-2 associated speckle protein
cGMP-PKG	Cyclic guanosine monophosphate-protein kinase G
PAM	Prototype adjacent motif
sgRNA	Single-guide RNA
qPCR	Real-time quantitative PCR

Supplementary Information

The online version contains supplementary material available at https://doi.org/10.1186/s12915-024-02029-2.

Additional file 1: Table S1 List of significantly downregulated pathways enriched in KEGG analysis from the comparative transcriptome of KO-*Td-JHAMT* vs. control. Table S2 List of significantly downregulated pathways enriched in KEGG analysis from the comparative transcriptome of KO-*Td-CYP15A1* vs. control. Table S3 List of significantly downregulated pathways enriched in KEGG analysis from the comparative transcriptome of KO-*Td-Met* vs. control. Table S4 List of significantly downregulated pathways enriched in KEGG analysis from the comparative transcriptome of KO-*Td-Kr-h1* vs. control. Table S5 List of significantly downregulated pathways enriched in KEGG analysis from the comparative transcriptome of KO-*Gb-Kr-h1* vs. control. Table S6 List of primers utilized in gRNA synthesis. Table S7 List of primers used for genotyping. Table S8 List of primers utilized in qPCR. Fig. S1 Timeline of *Thermobia domestica* embryogenesis, revealed by cellular dynamics, related to Fig. 1. Fig. S2 CRISPR/Cas9-mediated gene disruption. Fig. S3 The classification criteria and distribution of unhatched embryos resulting from knockout of *JHAMT*, *CYP15A1*, *Met*, or *Kr-h1* in *T. domestica*. Fig. S4 Embryonic phenotypes of class II and class I resulting from knockout of *JHAMT*, *CYP15A1*, *Met*, or *Kr-h1* in *T. domestica*. Fig. S5 KEGG enrichment analysis of the upregulated genes resulting from knockout of *JHAMT*, *CYP15A1*, *Met*, or *Kr-h1* in *T. domestica*. Fig. S6 Venn analysis of the downregulated genes resulting from knockout of *JHAMT*, *CYP15A1*, *Met*, or *Kr-h1* in *T. domestica*. Fig. S7 Comparative transcriptome analysis of the embryonic legs in *G. bimaculatus*.

Additional file 2: The individual data values for Figs. 1G, H, 2A, C, and 4A, B.

Acknowledgements

We thank the participants for taking part in this study.

Authors' contributions

S.L., Y.-X.L. and Y.B. conceived, designed, and led the project. Y.-N.L., M.Z. and Z.-Y.Y. performed most of the experimental work and analyzed the data. P.-Y.Z. and N.B. prepared part of the experimental materials for RNA-seq. D.-W.Y.

conducted bioinformatic data analysis. Y.B., Y.-X.L., and S.L. wrote the manuscript. All authors read and approved the final manuscript.

Funding
This research was supported by the National Natural Science Foundation of China to Y.B. (32300388), S.L. (32220103003 and 31930014), Y.-X.L. (32470443 and 32170425), and D.-W.Y. (32470542); the Postdoctoral Science Foundation (2022M721217); and the Guangdong Basic and Applied Basic Research Foundation (2022A1515110945) to Y.B.

Availability of data and materials
All data generated or analysed during this study are included in this published article, its supplementary information files and publicly available repositories. The RNA-seq data have been deposited in the China National Center for Bioinformation (accession number CRA016635, https://ngdc.cncb.ac.cn/gsa/search?searchTerm=CRA016635). The G. bimaculatus genome data can be accessed with the GenBank accession number GCA_017312745.1 [44]. The genome sequence of T. domestica can be obtained from the NCBI database (BioProject: PRJNA1149919, https://www.ncbi.nlm.nih.gov/bioproject/PRJNA1149919, with SRA accession numbers: SRR30683220, SRR30788026, and SRR30683218).

Declarations

Ethics approval and consent to participate
Not applicable.

Consent for publication
Not applicable.

Competing interests
The authors declare no competing interests.

Received: 1 June 2024 Accepted: 2 October 2024
Published online: 11 October 2024

References

1. Abdou MA, He Q, Wen D, Zyaan O, Wang J, Xu J, Wang J, et al. *Drosophila* Met and Gce are partially redundant in transducing juvenile hormone action. Insect Biochem Mol Biol. 2011;41:938–45.
2. Aboulafia-Baginsky N, Pener MP, Staal GB. Chemical allatectomy of late Locusta embryos by a synthetic precocene and its effect on hopper morphogenesis. J Insect Physiol. 1984;30:839–52.
3. Bai Y, Lv YN, Zeng M, Jia PY, Lu HN, Zhu YB, et al. Selection of reference genes for normalization of gene expression in *Thermobia domestica* (Insecta: Zygentoma: Lepismatidae). Genes (Basel). 2020;12:21.
4. Bai Y, Pei XJ, Ban N, Chen N, Liu SN, Li S, et al. Nutrition-dependent juvenile hormone sensitivity promotes flight-muscle degeneration during the aphid dispersal-reproduction transition. Development. 2022;149:dev200891.
5. Bai Y, Lv YN, Zeng M, Yan ZY, Huang DY, Wen JZ, et al. E93 is indispensable for reproduction in ametabolous and hemimetabolous insects. Development. 2024;22:dev.202518.
6. Barton LJ, Sanny J, Packard Dawson E, Nouzova M, Noriega FG, Stadtfeld M, Lehmann R. Juvenile hormones direct primordial germ cell migration to the embryonic gonad. Curr Biol. 2024;34:505–18.e6. https://doi.org/10.1016/j.cub.2023.12.033.
7. Belles X. The innovation of the final moult and the origin of insect metamorphosis. Philos Trans R Soc Lond B Biol Sci. 2019;374:20180415.
8. Belles X. Insect metamorphosis: from natural history to regulation of development and evolution. London: Academic Press; 2020.
9. Bitsch C, Baehr JC, Bitsch J. Juvenile hormones in *Thermobia domestica* females: identification and quantification during biological cycles and after precocene application. Experientia. 1985;41:409–10.
10. Brown JB, Boley N, Eisman R, May GE, Stoiber MH, Duff MO, et al. Diversity and dynamics of the Drosophila transcriptome. Nature. 2014;512:393–9. https://doi.org/10.1038/nature12962.
11. Chen N, Liu YJ, Fan YL, Pei XJ, Yang Y, Liao MT, et al. A single gene integrates sex and hormone regulators into sexual attractiveness. Nat Ecol Evol. 2022;6:1180–90.
12. Cruz J, Maestro O, Franch-Marro X, Martín D. Nuclear receptors EcR-A/RXR and HR3 control early embryogenesis in the short-germ hemimetabolous insect *Blattella germanica*. iScience. 2023;26:106548.
13. Daimon T, Uchibori M, Nakao H, Sezutsu H, Shinoda T. Knockout silkworms reveal a dispensable role for juvenile hormones in holometabolous life cycle. Proc Natl Acad Sci USA. 2015;112:E4226–35.
14. De Loof A, De Haes W, Janssen T, Schoofs L. The essence of insect metamorphosis and aging: electrical rewiring of cells driven by the principles of juvenile hormone-dependent Ca (2+)-homeostasis. Gen Comp Endocrinol. 2014;199:70–85.
15. Donoughe S, Extavour CG. Embryonic development of the cricket *Gryllus bimaculatus*. Dev Biol. 2016;411:140–56.
16. Erezyilmaz DF, Riddiford LM, Truman JW. Juvenile hormone acts at embryonic molts and induces the nymphal cuticle in the direct-developing cricket. Dev Genes Evol. 2004;214:313–23.
17. Fernandez-Nicolas A, Belles X. Juvenile hormone signaling in short germband hemimetabolan embryos. Development. 2017;144:4637–44.
18. Huang J, Marchal E, Hult EF, Tobe SS. Characterization of the juvenile hormone pathway in the viviparous cockroach. Diploptera punctata. PLoS One. 2015;10:e0117291.
19. Hou Y, Wang XL, Saha TT, Roy S, Zhao B, Raikhel AS, et al. Temporal coordination of carbohydrate metabolism during mosquito reproduction. PLoS Genet. 2015;11:e1005309.
20. Jindra M. Where did the pupa come from? The timing of juvenile hormone signaling supports homology between stages of hemimetabolous and holometabolous insects. Philos Trans R Soc Lond B Biol Sci. 2019;374:20190064.
21. Jindra M, Palli SR, Riddiford LM. The juvenile hormone signaling pathway in insect development. Annu Rev Entomol. 2013;58:181–204.
22. Jindra M, Bellés X, Shinoda T. Molecular basis of juvenile hormone signaling. Curr Opin Insect Sci. 2015;11:39–46.
23. Jindra M, Uhlirova M, Charles JP, Smykal V, Hill RJ. Genetic evidence for function of the bHLH-PAS protein Gce/Met as a juvenile hormone receptor. PLoS Genet. 2015;11:e1005394.
24. Jing YP, Wen X, Li L, Zhang S, Zhang C, Zhou S. The vitellogenin receptor functionality of the migratory locust depends on its phosphorylation by juvenile hormone. Proc Natl Acad Sci USA. 2021;118:e2106908118.
25. Kayukawa T, Minakuchi C, Namiki T, Togawa T, Yoshiyama M, Kamimura M, et al. Transcriptional regulation of juvenile hormone-mediated induction of Krüppel homolog 1, a repressor of insect metamorphosis. Proc Natl Acad Sci USA. 2012;109:11729–34.
26. Konopova B, Jindra M. Juvenile hormone resistance gene methoprene-tolerant controls entry into metamorphosis in the beetle *Tribolium castaneum*. Proc Natl Acad Sci USA. 2007;104:10488–93.
27. Leinwand SG, Scott K. Juvenile hormone drives the maturation of spontaneous mushroom body neural activity and learned behavior. Neuron. 2021;109:1836-1847.e5.
28. Liu P, Peng HJ, Zhu J. Juvenile hormone-activated phospholipase C pathway enhances transcriptional activation by the methoprene-tolerant protein. Proc Natl Acad Sci USA. 2015;112:E1871–9.
29. Liu S, Li K, Gao Y, Liu X, Chen W, Ge W, et al. Antagonistic actions of juvenile hormone and 20-hydroxyecdysone within the ring gland determine developmental transitions in *Drosophila*. Proc Natl Acad Sci USA. 2018;115:139–44.
30. Liu Y, Sheng Z, Liu H, Wen D, He Q, Wang S, et al. Juvenile hormone counteracts the bHLH-PAS transcription factors MET and GCE to prevent caspase-dependent programmed cell death in Drosophila. Development. 2009;136:2015–25.
31. Luo W, Liu S, Zhang W, Yang L, Huang J, Zhou S, et al. Juvenile hormone signaling promotes ovulation and maintains egg shape by inducing expression of extracellular matrix genes. Proc Natl Acad Sci USA. 2021;118:e2104461118.
32. Luxey M, Berki B, Heusermann W, Fischer S, Tschopp P. Development of the chick wing and leg neuromuscular systems and their plasticity in response to changes in digit numbers. Dev Biol. 2020;458:133–40.
33. Minakuchi C, Namiki T, Shinoda T. *Krüppel homolog 1*, an early juvenile hormone-response gene downstream of methoprene-tolerant, mediates

its anti-metamorphic action in the red flour beetle *Tribolium castaneum*. Dev Biol. 2009;325:341–50.
34. Naruse S, Washidu Y, Miura K, Shinoda T, Minakuchi C. Methoprene-tolerant is essential for embryonic development of the red flour beetle *Tribolium castaneum*. J Insect Physiol. 2020;121:104017.
35. Santos CG, Humann FC, Hartfelder K. Juvenile hormone signaling in insect oogenesis. Curr Opin Insect Sci. 2019;31:43–8.
36. Tian L, Guo E, Wang S, Liu S, Jiang RJ, Cao Y, et al. Developmental regulation of glycolysis by 20-hydroxyecdysone and juvenile hormone in fat body tissues of the silkworm. Bombyx mori J Mol Cell Biol. 2010;2:255–63.
37. Truman JW, Riddiford LM. The origins of insect metamorphosis. Nature. 1999;401:447–52.
38. Truman JW, Riddiford LM. The evolution of insect metamorphosis: a developmental and endocrine view. Philos Trans R Soc Lond B Biol Sci. 2019;374:20190070.
39. Truman JW, Riddiford LM, Konopova B, Nouzova M, Noriega FG, Herko M. The embryonic role of juvenile hormone in the firebrat, *Thermobia domestica*, reveals its function before its involvement in metamorphosis. Elife. 2024;12:RP92643.
40. Xie S, Shen B, Zhang C, Huang X, Zhang Y. sgRNAcas9: a software package for designing CRISPR sgRNA and evaluating potential off-target cleavage sites. PLoS ONE. 2014;9:e100448.
41. Wang X, Hou Y, Saha TT, Pei G, Raikhel AS, Zou Z. Hormone and receptor interplay in the regulation of mosquito lipid metabolism. Proc Natl Acad Sci USA. 2017;114:E2709–18.
42. Wen D, Rivera-Perez C, Abdou M, Jia Q, He Q, Liu X, et al. Methyl farnesoate plays a dual role in regulating *Drosophila* metamorphosis. PLoS Genet. 2015;11:e1005038.
43. Yamamoto K, Chadarevian A, Pellegrini M. Juvenile hormone action mediated in male accessory glands of *Drosophila* by calcium and kinase C. Science. 1988;239:916–9.
44. Ylla G, Nakamura T, Itoh T, Kajitani R, Toyoda A, Tomonari S, et al. Insights into the genomic evolution of insects from cricket genomes. Commun Biol. 2021;4:733.
45. Zheng H, Wang N, Yun J, Xu H, Yang J, Zhou S. Juvenile hormone promotes paracellular transport of yolk proteins via remodeling zonula adherens at tricellular junctions in the follicular epithelium. PLoS Genet. 2022;18:e1010292.
46. Zhu GH, Jiao Y, Chereddy SCRR, Noh MY, Palli SR. Knockout of juvenile hormone receptor, methoprene-tolerant, induces black larval phenotype in the yellow fever mosquito, *Aedes aegypti*. Proc Natl Acad Sci USA. 2019;116:21501–7.

Publisher's Note